Mikrochim. Acta 114/115, 33–52 (1994)

Mikrochimica Acta

Standardless X-Ray Analysis of Bulk Specimens

Jean-Louis Pouchou

O.N.E.R.A. Department of Materials, 29 Avenue de la Division Leclerc, F-92320 Chatillon, France

Abstract. The paper gives an overview of the problems of standardless analysis of bulk specimens by energy dispersive spectrometry (EDS) in scanning electron microscopes (SEM). The interest is concentrated on the present (and future) developments. The influence of the fluorescence excited by the continuum is discussed. Some improvements are proposed for the ionization cross-section. The difficulties due to the Coster-Kronig radiationless transitions are mentioned for the L lines. Emphasis is put on the necessity of an accurate modelling of the detector window, in order to be able to calculate reliably the efficiency of detection, mainly for the ultra-light elements. It is shown that some hypotheses such as the continuity of the fluorescence yield with the atomic number, which are currently accepted for heavier elements, could be wrong in the field of ultra-light elements. The capability of standardless analysis in special situations is discussed: analysis at oblique electron beam incidence, analysis of specimens with a thin conductive coating, analysis of stratified specimens.

Key words: EDS, X-ray microanalysis, standardless analysis, analytical scanning electron microscopy.

Although the highest quality procedure for X-ray microanalysis remains the analysis with standards by WDS spectrometry in the electron microprobe (EPMA), there is now a great demand for quick and reliable EDS procedures, since energy dispersive X-ray spectrometers (most often Si(Li) detectors) attached to scanning electron microscopes (SEM) are now representing the major part of the analytical systems in operation.

In principle, EDS spectrometry enables analysis with standards; but objectively, this mode of operation is not very effective with EDS systems, mainly because acquiring and processing the spectra of the standards is a long and tedious work. For most users, the need for quick answers is probably the main reason for their interest in standardless EDS analysis. But another reason is that EDS analysis with standards in the SEM comes up against some experimental difficulties:

—the main difficulty is that there is usually no beam current regulator in SEM columns. Some microscopes are really unstable, so that it is almost impossible to obtain a proper current stability ($\sim 1\%$) during a long sequence of standard and specimen spectra acquisition;
—in most scanning electron microscopes, there is no optical microscope to control easily, as in a microprobe, that the position of standards and specimen with

respect to the detector is strictly the same. An insufficient control of the take-off angle is a source of errors for strongly absorbed lines and low take-off angles;
—in the case of detectors with low aperture collimators (used to eliminate spurious X-rays) the surfaces of the specimen and of the standards have to be set rigorously in the same plane, to avoid errors due to different X-ray collimation rate;
—the operating conditions for the acquisition of the standard spectra have to be carefully controlled and adapted to avoid excessive counting rates, which could be the source of spectrum distortion by pulse piling up, mainly in the low energy region;
—although EDS systems of the new generation have an improved long-term stability compared to the older ones, it cannot be completely ruled out that during long experiments, some external perturbations (temperature change, vibrations, noise...) could alter the performance of the system (energy resolution and calibration of the spectra), thus leading to problems in further spectra processing.

In the usual EDS standardless procedures, all the elements present in the analyzed volume have to be declared and analyzed (either directly or by stoichiometry), the sum of the concentrations being essentially set to unity. The consequence is that any error in the analysis of one particular element, or any omission of undetectable element(s) may induce strong errors in the analytical output for the other elements. This has been a real danger with the old generation of beryllium window detectors, and this explains probably the suspicion of many analysts against standardless methods. Nowadays, with the recent detectors which can detect the ultra-light elements (starting from boron and sometimes from beryllium) and which have an improved spectral resolution, the danger of omitting a major element in much weaker. But the normalization of the concentrations implies that other errors may pass unremarked, in particular the errors coming from an improper description of geometry, or resulting from particular characteristics of the specimen (chemical heterogeneity, electrical charging...).

It would be a real improvement to have the capability in standardless procedures to check the reliability of the analysis, as it can be done in conventional analysis with standards by looking at the sum of the concentrations. To do that without standard, it would be necessary to have a perfect knowledge of all the fundamental physical parameters involved and of all the experimental parameters. This is unfortunately not realistic: the absolute values of the ionization cross-sections, for example, are far from being very well known, and are difficult to measure accurately; even the actual value of simple instrumental parameters, such as the effective solid angle of detection, may be out of user's knowledge. To overcome these limitations and obtain a reasonable compromise between speed and reliability, one could imagine for the future to promote procedures based on the measurement of a single standard used as universal reference for the experiment.

In the present paper, only standardless procedures will be considered. Methods involving hidden standards or libraries of standards will not be discussed.

Physical Basis

In the principle, the standardless procedure is not very different from the conventional technique with standards. Once the characteristic X-ray intensities of the

elements present in the specimen have been extracted from the specimen spectrum, the problem is to derive the k-ratios of these elements, as in conventional analysis. The difference here is that no standard spectra have been acquired, so that for every element i the k-ratio has to be formed by dividing the experimental intensity by the computed intensity of the corresponding pure element standard:

$$k_i = \frac{I_i^{exp}}{I_{istd}^{calc}}. \tag{1}$$

In the ZAF notation, the theoretical intensity of a pure standard can be written as:

$$I_{istd}^{calc} = n^{e^-} \cdot \frac{\Omega}{4\pi} \cdot \varepsilon_d \cdot \omega_j \cdot p_{jl} \cdot (1 + f_c) \cdot (1 + g_{ck}) \cdot f(\chi) \cdot \frac{N^o}{A} \cdot R \cdot \int_{E_o}^{E_j} \frac{Q_j(E)}{dE/d\rho s} \cdot dE. \tag{2}$$

In a $\phi(\rho z)$ approach, the same quantity can be expressed by the following equation, which additionally includes the effect of tilting the specimen:

$$I_{istd}^{calc} = n^{e^-} \cdot \frac{\Omega}{4\pi} \cdot \varepsilon_d \cdot \omega_j \cdot p_{jl} \cdot (1 + f_c) \cdot (1 + g_{ck}) \cdot \frac{N^o}{A} \cdot \frac{Q_j(E_0)}{\cos(\beta)} \cdot \int_0^{R_{max}} \Phi(\rho z) \cdot \exp(-\chi \cdot \rho z) \cdot d\rho z. \tag{3}$$

The following notations are used:
n^{e^-} is the number of incident electrons;
Ω is the solid angle of detection;
ε_d is the efficiency of the detector (including the yield of the detector crystal itself and the transmission through the window and coatings);
ω_j is the fluorescence yield of the level j;
p_{jl} is the relative probability of the transition from the particular outer level l to the ionized level j, leading to the line of interest;
f_c represents the fraction of the intensity due to secondary fluorescence excited by the continuum (for a pure standard, the fluorescence by lines is negligible);
g_{ck} represents the contribution of the Coster-Kronig radiationless transitions between subshells to the ionization on level j (g_{ck} is zero for the K lines);
χ is the absorption factor, which is the product of the mass absorption coefficient μ/ρ by the cosecant of the take-off angle θ,
$f(\chi)$ is the absorption correction factor of the ZAF approach;
N^o is the Avogadro's number;
A is the atomic mass;
R is the backscattering factor (1-R represents the loss of ionization due to the backscattered electrons);
E_0 is the energy of incident electrons;
E_j is the critical energy of level j;
$Q_j(E)$ is the ionization cross-section of level j by electrons with energy E;
$dE/d\rho s$ is the electron energy loss equation;
ρs is the electron path (in mass units); ρz is the mass depth;
β is the specimen tilt angle;
$\Phi(\rho z)$ is the distribution in depth of the primary ionization on level j;
R_{max} is the upper limit of integration of $\Phi(\rho z)$, equal to the ultimate ionization

depth R_x in the case of the PAP model, and equal to infinity in the case of $\Phi(\rho z)$ models with exponential or gaussian tails (XPP or gaussian model).

In practice, the k-ratios obtained by comparing experimental spectra with computed standard intensities may have no absolute meaning, for example if the beam current is not taken into account in the standardless procedure, or if the procedure uses a value for the detection solid angle which is not the real value for the particular detector. Hence, it is frequent that the k-ratios displayed by the standardless programs are the normalized values which are used as concentrations of first approximation in the first loop of the "correction" procedure.

The "correction" procedure is not different from that of usual analysis with standards. In the same manner, the iteration is stopped when all the concentrations become stationary. Since any absolute error on a particular element produces an error of the same amplitude on the sum of the others, it is obvious that there is a great advantage to incorporate into standardless procedures the best models available, i.e. reliable $\phi(\rho z)$ models, rather than the approximations used in ZAF procedures. In that way, significant improvements can be obtained in the analysis of light and ultra-light elements, in the analysis at oblique beam incidence, in the analysis of coated specimens, and even more generally in the analysis of stratified specimens.

Fluorescence by the Continuum

Most procedures for quantitative X-ray analysis with standards take into account the effects of the fluorescence exited by lines, but neglect the fluorescence excited by the continuum. However, the results are generally considered as being satisfactory. The reason is that the contribution of the fluorescence by the continuum is generally not very high, and that the effects are of the same order of magnitude in the specimen and in the standard (provided that the atomic numbers and absorption coefficients are not too different), so that they compensate more or less each other when forming the k-ratios. But in the case of standardless analyses, such a compensation does not exist. For all the analytical lines, there is actually in the experimental spectrum a contribution of fluorescence by the continuum. This contribution is weak for soft X-rays, but stronger for high energy lines. Hence, this fluorescence by the continuum definitely has to be taken into account in the theoretical standard intensity used to form the k-ratio.

Figure 1 shows the contribution of the fluorescence by the continuum (relative to the primary intensity) computed for Kα and Lα lines of pure targets at 30 kV. At 35° take-off, it represents $\sim 5\%$ for Zn Kα ($Z = 30$; $h\nu = 8.4$ keV) and more than 20% for Mo Kα ($Z = 42$; $h\nu = 17.5$ keV). For the L lines, it is close to 5% for W Lα ($Z = 74$; $h\nu = 8.4$ keV) and exceeds 14% for U Lα ($Z = 92$; $h\nu = 13.6$ keV). For the M lines, it is always less than 1.5%.

The full computation of the fluorescence by the continuum, applied to the standards and to all the analytical lines of the specimen spectrum, is long compared to the other parts of the calculation (atomic number and absorption effects). Considering the other sources of uncertainty in the standardless procedure, one can wonder if a full computation of the fluorescence by continuum is really necessary. In fact, a simplified approach can be effective. In this simplified approach, the fluorescence by the continuum is computed for the pure standards only, so that the k-ratios

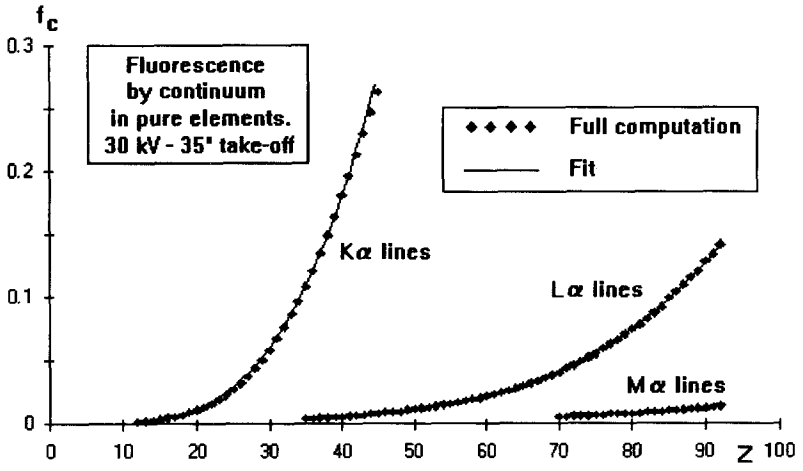

Fig. 1. Fluorescence by continuum relative to the primary intensity computed for pure element standards at 35° take-off

formed by dividing the experimental specimen intensities by the computed standard intensities are meaningful and basically, they are equivalent to k-ratios which would be measured with real standards. Then, these k-ratios can be processed without taking into account the fluorescence by continuum, as it is conventionally done in most ZAF or $\phi(\rho z)$ correction procedures with standards. In that way, the computation of the fluorescence by the continuum is restricted to the main lines of pure elements. The corresponding mass absorption coefficients being known, it is possible to further simplify and speed up the practical procedure by using an empirical fit of the relative fluorescence intensity instead of the theoretical computation.

For the Kα lines of pure elements, the following expression, which can be used up to Z = 47, satisfactorily fits the results of the theoretical computation:

$$f_c = \frac{I_{fc}}{I_{istd}^{calc}} = \frac{G}{\text{cosec}^p(\theta)} \tag{4}$$

with

$$G = -2.8566\ 10^{-3} + Z\cdot[1.6492\ 10^{-3} + Z\cdot(-1.8\ 10^{-4} + 6.7086\ 10^{-6}\cdot Z)] \tag{5a}$$

and

$$p = 0.3\ \{1 - \exp[1.3(1 - Z/20)]\} \tag{5b}$$

For the Lα lines, the following fit can be used starting from Z = 30:

$$G = -9.370\ 10^{-2} + Z\cdot[5.992\ 10^{-3} + Z\cdot(-1.2937\ 10^{-4} + 1.02495\ 10^{-6}\cdot Z)] \tag{6a}$$

and

$$p = 0.3\ \{1 - \exp[2.52(1 - Z/49)]\} \tag{6b}$$

For the Mα lines, the following fit can be used for Z > 70::

$$G = 3.326\ 10^{-2} + Z\cdot[-1.01\ 10^{-3} + 8.5827\ 10^{-6}\cdot Z)] \tag{7a}$$

and

$$p = -3.2175 + 6.344\ 10^{-2}\ Z - 3.2286\ 10^{-4}\ Z^2 \qquad (7b)$$

In practice, the influence of the accelerating voltage on the fluorescence by continuum can be neglected. For all lines which are not strongly absorbed in the pure element, the contribution of the excitation by continuum relative to the primary emission is almost independent of the voltage. In the case of the Lα line of element Re for example ($Z = 75$, $\mu/\rho \sim 150$ cm^2/g), the ratio of secondary to primary emission is ~5.5% at 30 kV and ~5.75% at 15 kV. For elements emitting soft lines, which are more strongly absorbed, the effect of the voltage becomes higher, but has no practical influence, because the secondary emission is much weaker: for example, in the case of the Lα line of Rh ($Z = 45$, $\mu/\rho \sim 570$ cm^2/g), the ratio of secondary to primary emission varies from 0.83% at 30 kV to 0.58% at 5 kV.

$\phi(\rho z)$ Model and Ionization Cross-Section

The $\phi(\rho z)$ model by itself is certainly the part of the standardless procedure which produces the smallest uncertainties. Models such as PAP and XPP [1], as well as other formulations derived from the original Packwood and Brown's gaussian model [2, 3], are known to give reliable results when they are applied to analyses with standards. Some of them have been shown to predict very correctly the variation with the accelerating voltage of the emerging intensity, in a wide voltage range, and in a wide range of X-ray energies [4]. In this respect, we believe that an ionization cross-section varying with the overvoltage ratio U as $\ln(U)/U^m$, with $m < 1$, is more satisfactory than the conventional expression used in many ZAF procedures which corresponds to $m = 1$. One has to be aware that in standardless analysis, the variation of the ionization cross-section with U has a much stronger influence than in conventional analysis with standards. With standards, the ionization cross-section is only involved in the atomic number correction for the computation of the retardation factor (i.e. the integral in Eq. (2)). During this process, the errors from inaccuracies in the cross-section cancel almost completely when forming the ratio of these factors for the unknown and the standard. On the opposite, the ionization cross-sections have in standardless analysis a direct influence on the evaluation of the k-ratios. Consequently, any inaccuracy in the shape of the cross-sections is a source of errors. These errors are maximum for specimens containing major elements submitted to widely different overvoltage ratios (for example, in a specimen containing Mo and Al, the overvoltage ratio at 30 kV would be low (~1.5) for the Mo Kα line and high (~20) for the Al Kα line).

The other major problem in the standardless procedures is the knowledge of the coefficient B_j in the expression of the ionization cross-section:

$$Q_j = B_j \cdot z_j \cdot \frac{\ln(U)}{E_j^2 \cdot U^m} \qquad \text{with } U = \frac{E}{E_j} \qquad (8)$$

(z_j is the number of electrons on the ionized shell or subshell).

Conventionally, it is assumed that for a given level, the coefficient B_j has the same value for all the elements. It is also generally assumed that the fluorescence yield ω_j varies continuously with the atomic number of the emitting element. Consequently, if the ionized level is not splitted (case of K lines) so that there is no

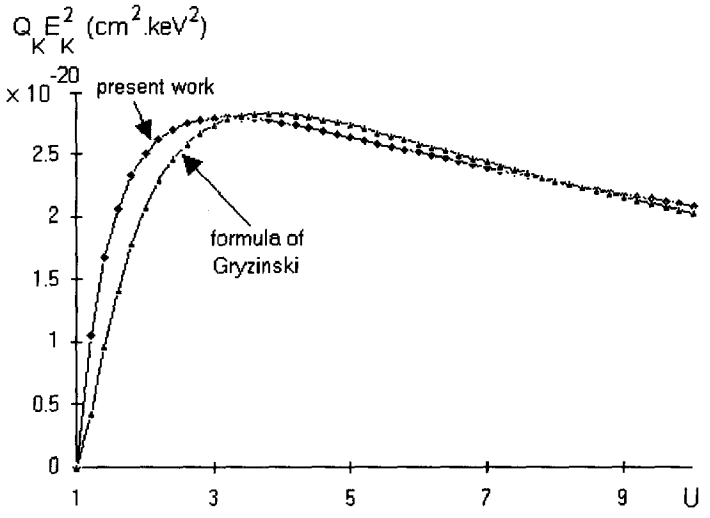

Fig. 2. Comparison of the ionization cross-section of Eq. (9) with the expression of Gryzinski

possibility for an ionization transfer between subshells, the primary intensity should vary smoothly from an element to the next one. One has to be aware that this basic assumption could actually be wrong, mainly in the field of ultra-light elements.

The experimental determinations of the ionization-cross section reported for K levels are globally consistent, and indicate that the quantity $Q_j \cdot E_j^2$ is almost identical for all the elements and reaches the same maximum value ($\sim 2.8\ 10^{-20}$ cm$^2 \cdot$ keV^2) for an overvoltage value between 2 and 3. We use this as a basic property to express the K ionization cross-section as follows:

$$Q_K = 1.4\ 10^{-20} \cdot z_K \cdot \exp(1) \cdot m \cdot \frac{\ln(U)}{E_K^2 \cdot U^m} \qquad (Q_K \text{ in cm}^2,\ E_K \text{ in keV}) \tag{9}$$

with $z_K = 2$ and m defined as [1]:

$$m = 0.86 + 0.12 \exp[-(Z/5)^2] \tag{10}$$

As shown in Fig. 2, the cross-section of Eq. (9) is very similar to the widely used Gryzinski expression in the intermediate range of overvoltage ratios (U $\sim$ 4 to 10), but predicts higher values at low overvoltage.

Recently, on the basis of standardless experiments involving measurements at very low overvoltage (U less than 1.2) on homogeneous and on layered specimens, we realized that Eq. (9) was not fully satisfactory in this domain: we observed that for the elements analyzed without standards at very low overvoltage, the computed concentrations were systematically found to be higher than the nominal ones, by up to 20% in certain cases (Cu Kα at 10 kV). This means that the corresponding k-ratios are too high, i.e. that the intensity of the corresponding pure standards are too low at very low overvoltage. For this reason, we have added two corrective terms to Eq. (9), in order to increase the ionization cross-section for U values close to 1.

$$Q_K = 1.4\ 10^{-20} \cdot z_K \cdot \exp(1) \cdot m_1 \cdot \sum_{i=1}^{3} a_i \frac{\ln(U)}{E_K^2 \cdot U^{m_i}} \tag{11}$$

with

$$\begin{aligned} a_1 &= 1 \qquad m_1 \text{ given by equation 10} \\ a_2 &= 0.1 \qquad m_2 = 5 \\ a_3 &= 1.5 \qquad m_3 = 30 \end{aligned} \tag{12}$$

The modification of the ionization cross-section due to the additional terms is shown in Fig. 3. Table 1 shows the typical improvement obtained by applying Eq. (11) instead of Eq. (9), in the case of GaP.

For the L shells, the values reported for the L_3 ionization cross-sections are more scattered. For the moment, we have adopted in our standardless procedure an

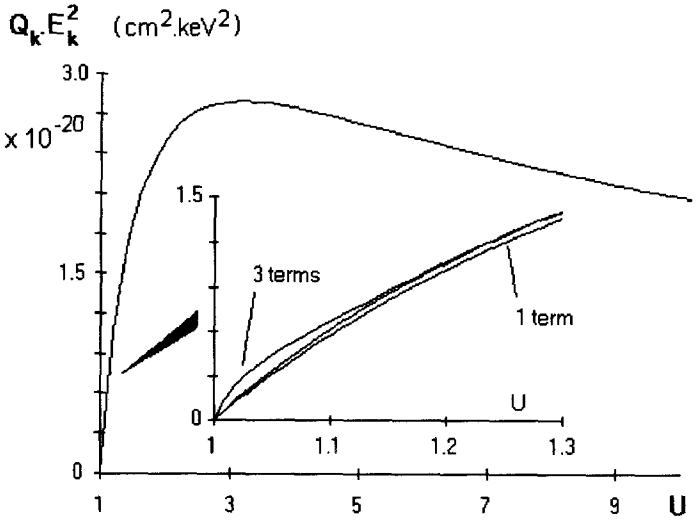

Fig. 3. Influence of additional terms in the expression of the ionization cross-section at very low overvoltage

Table 1. Standardless results obtained for GaP at several voltages using the modified expression of the ionization cross-section (Eq. (11)) and the old one (Eq. (9))

	Overvoltage ratio		k-ratio (%)		With modified Q_K atom %		With old Q_K atom %	
kV	Ga Kα	P Kα	Ga Kα	P Kα	Ga	P	Ga	P
12	1.16	5.60	63.31	25.22	49.47	50.53	53.01	46.99
15	1.45	7.00	63.95	21.95	49.55	50.46	50.82	49.18
20	1.93	9.34	64.12	17.69	49.15	50.85	49.67	50.33
25	2.41	11.67	64.91	13.93	49.66	50.34	49.94	50.06
30	2.89	14.01	65.21	11.31	49.78	50.22	49.91	50.09
Average					49.52	50.48		
Relative r.m.s.					0.4%	0.4%		
Dev. from nominal					−1%	+1%		

average value of B_j corresponding to a maximum value of 4.8 10^{-20} $cm^2 \cdot keV^2$ for $Q_j \cdot E_j^2$:

$$Q_{L3} = 1.2\ 10^{-20} \cdot z_{L3} \cdot \exp(1) \cdot m \cdot \frac{\ln(U)}{E_{L3}^2 \cdot U^m} \tag{13}$$

with $z_{L3} = 4$ and $m = 0.82$ [1].

The above value of B_j for L lines still remains uncertain because the situation is complicated by the non-radiative Coster-Kronig transitions between subshells.

Coster-Kronig Radiationless Transitions

In the case of L and M lines, the populations of vacancies produced on the subshells by direct ionizations are altered by the radiationless Coster-Kronig transitions between subshells. For example, in the case of the Lα line, the initial vacancy population in the L_3 shell is increased by a transfer of ionizations originating from the L_1 and the L_2 levels. The g_{ck} term of Eqs. (2) and (3) can be written for the L_3 shell:

$$g_{ck} = f_{13} \cdot \frac{N_1}{N_3} + f_{23} \cdot \left(\frac{N_2}{N_3} + f_{12} \cdot \frac{N_1}{N_3} \right), \tag{14}$$

where f_{ij} are the Coster-Kronig transition probabilities from subshell i to subshell j, and N_1, N_2, N_3 are the direct vacancy populations of subshells L_1, L_2, L_3. In the situations where the overvoltage ratios would be very high for all the elements (as it can be in transmission electron microscopy), N_1, N_2 and N_3 would be the statistical weights of L_1, L_2 and L_3, i.e. respectively 2, 2 and 4. In the voltage range of SEM or EPMA, the overvoltage is not high in many cases, so that it should be taken into account that the subshells with different critical energy E_j are not excited with the same efficiency. The differences in the backscattering factors being negligible in practice, the N_j terms can be identified to the retardation factors 1/S:

$$N_j \propto \frac{1}{S} = \int_{E_0}^{E_j} \frac{Q_j(E)}{dE/d\rho s} \cdot dE. \tag{15}$$

The values of the Coster-Kronig transition probabilities to be used in practice are a real source of trouble. There is a strong uncertainty in the reported data [5], and it is difficult to extract from the reported data a reliable fit because the variations of these transition probabilities with the atomic number are essentially discontinuous. From the literature, it seems that the f_{23} factor is probably not a strong source of errors because it is not very high (less than 0.2) and does not vary strongly in a wide range of atomic number ($Z \sim 37$ to 90). The f_{12} factor appears to have more pronounced variations: it is typically equal to ~ 0.25 for $Z \sim 30$ to 40, decreases down to ~ 0.05 for elements with Z between 40 and 50, increases again up to ~ 0.2, and finally decreases again for elements with Z higher than ~ 75. But since the effect of f_{12} is attenuated by f_{23}, its influence is probably not critical. The major source of errors comes from the transitions from L_1 to L_3, caracterized by the f_{13} probability. The theory predicts high values for f_{13}, with strong discontinuities as a function of Z (from ~ 0.3 to ~ 0.7 and may be more).

Figure 4 gives the theoretical curves corresponding to the data proposed by Bambynek et al. [5]. On the same figure, some isolated values are plotted, repre-

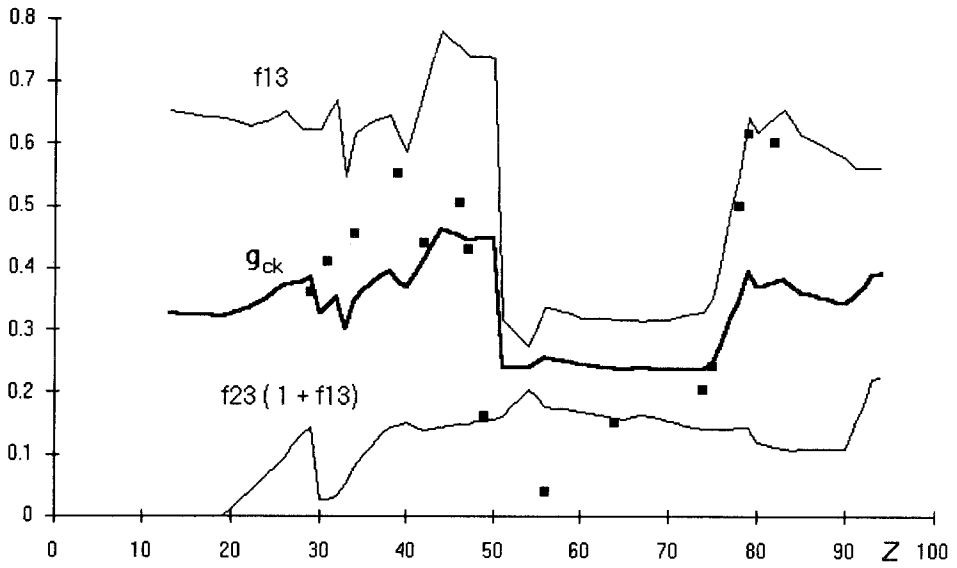

Fig. 4. Increase of the L_3 vacancy population due to the Coster-Kronig transitions. The g_{ck} curve is computed using the data of Bambynek et al. [5]. The dots are the values derived from standardless analyses

senting the relative number of ionizations that should be added to the direct L_3 ionizations in order to obtain satisfactory standardless analyses (the specimens of known composition used for this cross-check were Au-Cu, Au-Pd, Co-Pt, Pt-V, Mo-Re, W-Re, Ag-Y-Gd, Ba-Fe-O, Y-Ba-Cu-O, Y-Fe-O, Pb-Se, Ga-Se and Ga-P compounds). Obviously, these empirical values exhibit a variation with Z which is strongly correlated with the theoretical g_{ck} factor, but their range of variation is significantly greater than that of g_{ck}. While studying the Lα intensities of pure standards, Labar [6] also found deviations between experimental results and theoretical predictions. He suggested that the observed discrepancy could be due to B_j coefficients (Eq. (8)) higher for the L_1 and the L_2 levels than for the L_3 level. This would increase the influence of the Coster-Kronig transitions for all elements. Since our data indicate that the effect of the radiationless transitions should be lower for the elements of the medium range of atomic numbers ($Z \sim 50$ to 75), and higher for the other elements, we believe that the explanation is more probably that the values of the theoretical Coster-Kronig probabilities are not fully satisfactory.

To conclude this paragraph, it can be asserted that for lines other than K lines, the effect of the Coster-Kronig transitions definitely needs to be taken into account in the standardless computations. In the case of the Lα line, the Coster-Kronig transitions are weak for elements in the atomic number range 50–75, but may enhance the Lα emission of the other elements by more than 50%. This explains that standardless programs which do not take into account the Coster-Kronig transitions and are based on smooth adjustments of the physical parameters governing the generated intensity may lead to errors exceeding 25% for some elements. The use of the theoretical Coster-Kronig probabilities globally improves significantly the reliability of standardless analyses, but there is still a need for an empirical adjustment to obtain an accuracy comparable to that of the analysis with standards.

Detection Efficiency

The EDS detectors of the old generation were protected by a beryllium window, which was absorbing completely the soft X-rays emitted by the ultra-light elements. In principle, the computation of the window and detector efficiency was easy, by use of the relation:

$$\varepsilon_d = \exp[-(\mu/\rho)_{Be} \cdot \rho t_{Be}] \cdot \exp[-(\mu/\rho)_{Au} \cdot \rho t_{Au}] \cdot \exp[-(\mu/\rho)_{Si} \cdot \rho t_{Si}] \cdot \{1 - \exp[-(\mu/\rho)_{Si} \cdot \rho T_{Si}]\}. \quad (16)$$

The factors in Eq. (16) are respectively the transmission through the Be window, the transmission through the detector coating, the transmission through the detector dead layer, and the absorption inside the solid-state detector itself. In practice, the determination of the actual detector efficiency was not as easy as expected, mainly because the Be window was generally found to have a mean thickness much higher than the nominal one, a strong heterogeneity, and was sometimes covered with a grease layer to avoid porosity.

The detectors of the new generation have atmospheric pressure-resistant ultra-thin windows, which enable to detect the ultra-light elements. These windows are high technology products, with chemical and geometrical characteristics which can be reliably controlled. The metallic coatings of the window and of the detector can also be controlled by the manufacturer. The most questionable parameter is the dead layer, firstly because the concept of a uniform layer with a zero conversion efficiency located at the detector surface is certainly an oversimplified view, and secondly because the appropriate value to be used for this parameter in a program can only be estimated by comparing the sensitivity for boron and carbon (because the B K line is much more strongly absorbed in Si than the C K line, as can be seen from Table 2). Since this determination also involves a theoretical computation of the emitted intensities, the resulting value of the dead layer parameter greatly depends on the hypotheses governing the theoretical computation in this low energy range (mainly the use of a constant value for B_j in the cross-section and the use of a fluorescence yield varying smoothly with Z).

Table 2. Transmission factors of individual parts of a typical Super Quantum detector for several K lines in the low energy region

	Thickness	B 185 eV	C 282 eV	N 392 eV	O 523 eV	Al 1487 eV	Ti 4510 eV
Thin window	250 nm	66.8%	19.8%	45.7%	54.8%	87.7%	99.3%
Thick regions		17%	3%	7%	11%	57%	98%
Window coating	15 nm	77.2%	88.2%	94.6%	97.2%	99.8%	99.9%
Detector coating	20 nm	51.8%	72.3%	84.7%	91.3%	92.2%	99.6%
Si dead layer	40 nm	47.4%	70.8%	86.7%	92.1%	99.5%	99.7%
	100 nm	15.5%	42.2%	68.1%	81.5%	98.8%	99.2%
C contamination	50 nm	93.5%	97.8%	77.5%	88.3%	99.3%	100%
	100 nm	87.4%	95.8%	60.0%	78.0%	98.6%	99.9%

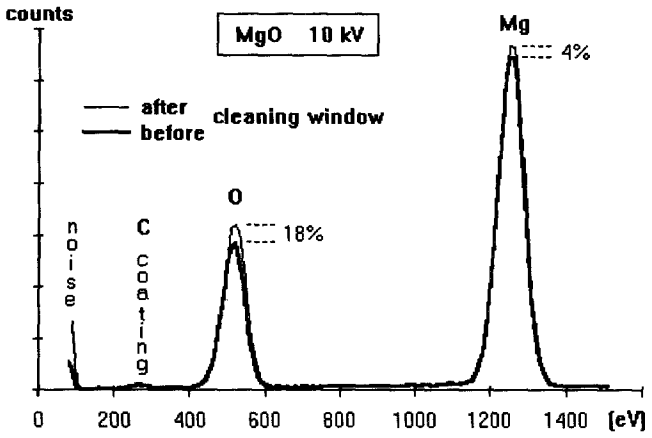

Fig. 5. Comparison of MgO spectra collected before and after cleaning the window of the Super Quantum detector

Obviously, an accurate parameterization of the window and of the near-surface region of the detector is particularly important for the ultra-light elements. Additionally, it should not be omitted that in this low energy range, any contamination of the window (or of the detector crystal) is a source of significant errors. The example of Fig. 5 shows for a MgO specimen the increase of the ratio O Kα/Mg Kα obtained by cleaning with freon the window of a Super Quantum detector, after 6 months operation in a SEM equipped with a turbomolecular pump. Assuming that the contamination is principally carbon, such a sensitivity change would correspond to a carbon thickness of $\sim$80 nm.

Depending on the manufacturer, there are different technologies for the window, but in all the cases, the ultra-thin window has to be supported by thicker material, to be pressure-resistant. Depending on the type of window, the thick material can be of the same nature as the thin material or of a different nature. In all cases, the chemical and geometrical characteristics of these thick regions have also to be properly defined, since they may partially transmit some of the radiation in the high energy region. Obviously, the standardless programs should use for computing the detector efficiency a correct description of the actual nature of detector and window. The problem in this field is that manufacturers may keep secret some aspects of their system. The consequence is that some software programs written independently of the manufacturers may use parameters which do not agree with the actual detector characteristics.

Table 2 gives transmission factors for soft X-rays in the case of a typical Kevex Super Quantum detector, the major constituent of the window being boron. In practice, every detector has to be provided with its own characteristic parameters, which can be different from one batch to another.

Software Adaptation for the Ultra-Light Elements

Once the modelling of the window has been done with the maximum care (this is an essential condition of success), one has to find out the values of the fluorescence yield ω_K giving the best agreement with the experiments. Some currently accepted

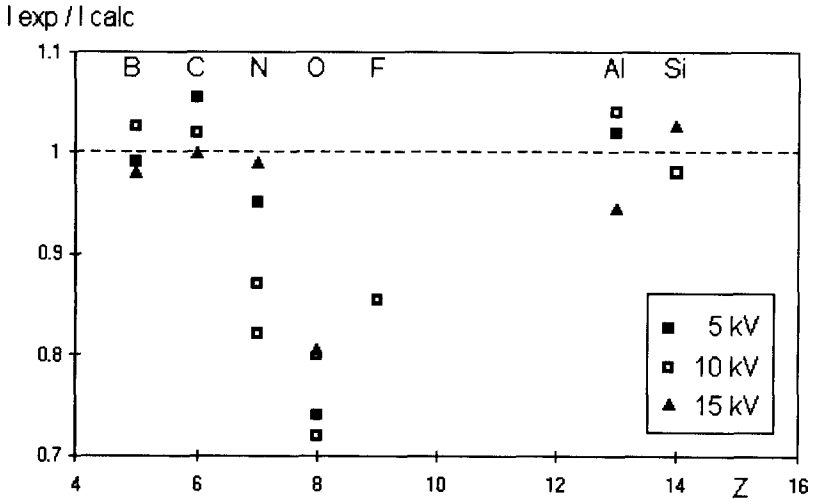

Fig. 6. Ratio of the experimental intensity to the intensity calculated with the assumption of a smooth variation of the fluorescence yield adjusted on B, Si and heavier elements

values for ω_K have been proposed by Bambynek et al. [5] and Krause [7]. Both sets of data are in satisfactory agreement for light to heavy elements, but differ significantly (sometimes by a factor of 2) for the ultra-light elements. Assuming that the emitted intensity varies continuously with the atomic number, it is possible to obtain an expression of the fluorescence yield such that the X-ray intensities computed for the lightest elements (B, C) and for heavier elements (Al, Si, ...) are in good agreement with the intensities measured on standards (Fig. 6).

But it can be seen in Fig. 6 that with such assumptions, the intensities measured for intermediate elements (N, O, F) are lower than the calculated ones, mainly in the case of oxygen. The discrepancy observed for oxygen and fluorine could be the

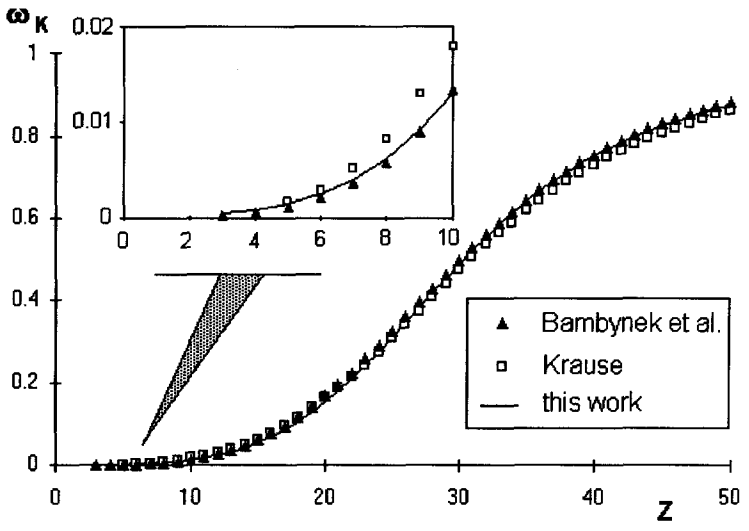

Fig. 7. Comparison of Eq. (17) of the K fluorescence yield with published data

result of a preferential absorption by carbon. If one assumes that the detector crystal is contaminated with a carbon layer, the consistency between experimental and computed intensities is obtained for B, C, O, F (to a lower extent), Al, Si and heavier elements with a thickness of the detector contamination equal to 95 nm carbon and with the following expression of the fluorescence yield:

$$\omega_K = Y^4/(1 + Y^4)$$

with

$$Y = 0.06893861 + Z[0.024152 + Z(3.324179\ 10^{-4} - 3.92704544\ 10^{-6}\ Z)]. \quad (17)$$

Figure 7 shows that in the field of ultra-light elements and in the field of medium Z elements, Eq. (17) is between the values proposed by Krause [7] and the values

Table 3. Results of standardless analyses of a titanium carbide (nominal 18.2 wt% C) at varying voltage. Super Quantum EDS detector. Quantex+/XPP program. Take-off 35°

Voltage (kV)	k-ratio		Weight%	
	Ti	C	Ti	C
10	0.7667	0.1230	81.75	18.25
15	0.7732	0.0903	81.60	18.40
20	0.7896	0.0697	82.49	17.51
Average			81.95	18.05
Relative r.m.s.			0.48%	2.16%
Relative deviation from nominal			+0.2%	−0.8%

Table 4. Results of standardless analyses of a nickel monoxide $Ni_{51}O_{49}$ (atomic composition obtained by EPMA at 15 kV) at varying voltage. Super Quantum EDS detector. Quantex+/XPP program. Take-off 35°

Voltage (kV)	k-ratio		Atom %	
	Ni	O	Ni	O
15	0.7479	0.1234	50.72	49.28
20	0.7619	0.0944	51.68	48.32
25	0.7702	0.0780	52.13	47.87
30	0.7760	0.0687	52.34	47.66
Average			51.72	48.29
Relative r.m.s.			1.2%	1.3%
Relative deviation from nominal			+1.4%	−1.5%

corresponding to the expression of Bambynek et al. [5]; the proposed equation is slightly below the comparison data for the light elements. Tables 3 and 4 give examples of the good results which can be obtained by standardless analysis in the case of compounds containing carbon and oxygen.

Unfortunately, it is obvious that the effect of a contamination of the detector by carbon is maximum for the radiation of nitrogen. As can be seen in Fig. 6, our intensity measurements for nitrogen are more strongly scattered than for other elements (this is due to a low nitrogen concentration in the Cr_2N standard, to the presence of an Al coating in the BN standard, to the influence of the contamination in both cases). But these measurements indicate that the hypotheses which give satisfactory results for the other elements would produce in the case of nitrogen a computed intensity too low by 20 to 30% (Table 2 shows that the absorption of N Kα in the carbon layer would be $\sim$40%).

To summarize, the hypotheses that we have temporarily adopted (same value of B_j for all the elements, continuous variation with Z of the fluorescence yield, contamination of the detector by carbon) permit to obtain satisfactory standardless results for the ultra-light elements (starting from boron), except in the case of nitrogen. More measurements, performed with different systems, are required to clarify the situation. In the present state, we have the feeling that for the ultra-light elements, either the B_j factor in the ionization cross-section should not be constant or the fluorescence yield ω_K should not vary smoothly from an element to the next one. However, the modifications which could be done in the equation of the fluorescence yield should keep almost unchanged the ω_K values from light to heavy elements.

Tilted Specimens

It may be useful in a scanning electron microscope to tilt the specimen by an angle β, either to improve the secondary electron detection or for other reasons related to the particular geometry of the specimen. In tilted situations, the conventional quantitative procedure are not able to describe properly the effects on the emerging intensity. There is actually a competition between two phenomena: a loss of primary ionizations due to the increasing number of backscattered electrons, and a modification of the absorption of the radiation in the specimen. The absorption effect itself is the result of two phenomena: a reduction of the mean depth of ionization which tends to reduce the absorption, and a variation of the take-off angle, which also reduces the absorption in the cases where the specimen is tilted towards the detector, but increases the absorption in the other cases.

The XPP model seems to be presently the only $\phi(\rho z)$ model which takes into account the effects described above. Figure 8 shows the modifications of the $\phi(\rho z)$ function under influence of tilt in the case of Al Kα radiation in NiAl. The $\phi(\rho z)$ functions here are defined with respect to an inclined isolated self-supported film, so that the primary generated intensity is represented by the area of $\phi(\rho z)$ divided by $\cos(\beta)$. Table 5 gives the results of standardless analysis obtained in the case of NiAl from 0 to 70° tilt. In the present geometry, the angle of azimuth is such that tilting the specimen produces an increase of the take-off angle, and consequently a significant increase of the Al Kα intensity.

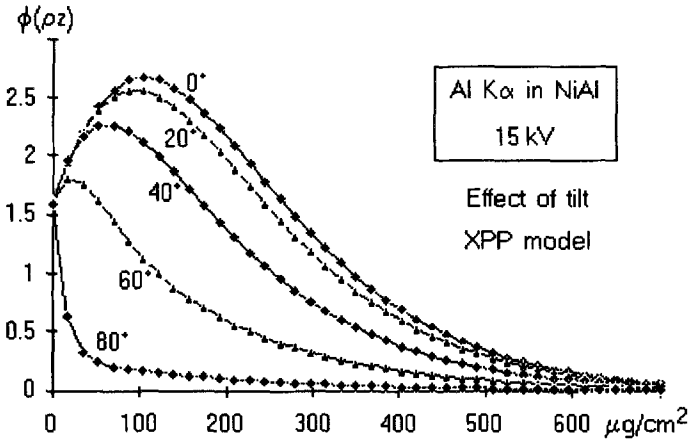

Fig. 8. Influence of tilt on the $\phi(\rho z)$ function in the XPP model. Case of Al Kα radiation in NiAl at 15 kV

Table 5. Results of standardless analysis of a NiAl compound (nominal 30.92 wt % Al) at varying tilt angle. 15 kV. Azimuth 45°

Tilt (deg)	Take-off (deg)	k-ratio		Weight %	
		Ni	Al	Ni	Al
0	30.0	65.83	14.94	68.80	31.20
10	38.5	67.16	16.13	70.05	29.95
20	46.6	66.66	17.99	69.53	30.47
30	53.9	67.94	18.37	70.66	29.34
40	59.9	66.13	20.67	68.82	31.18
50	63.6	66.19	21.48	68.73	31.27
60	64.1	65.97	22.33	68.35	31.65
70	61.1	65.50	23.23	67.73	32.27
Average				69.08	30.92
Relative r.m.s.				1.3%	2.8%
Relative deviation from nominal				0%	0%

Coated Specimens

To avoid charging and beam deflection in a microprobe or a SEM, the non conductive specimens have to be coated to have a fixed surface potential. (It should be pointed out that this does not eliminate the fact that the electric field inside the specimen may distort the $\phi(\rho z)$ functions and consequently produce errors in the quantification of strongly absorbed radiation). Very frequently, carbon coatings in the range 10–30 nm are used for microanalysis experiments. Some authors prefer to use gold, which has to be in very thin layers (a few nm). As opposed to the case of analysis with standards, the influence of the coating does not vanish when forming

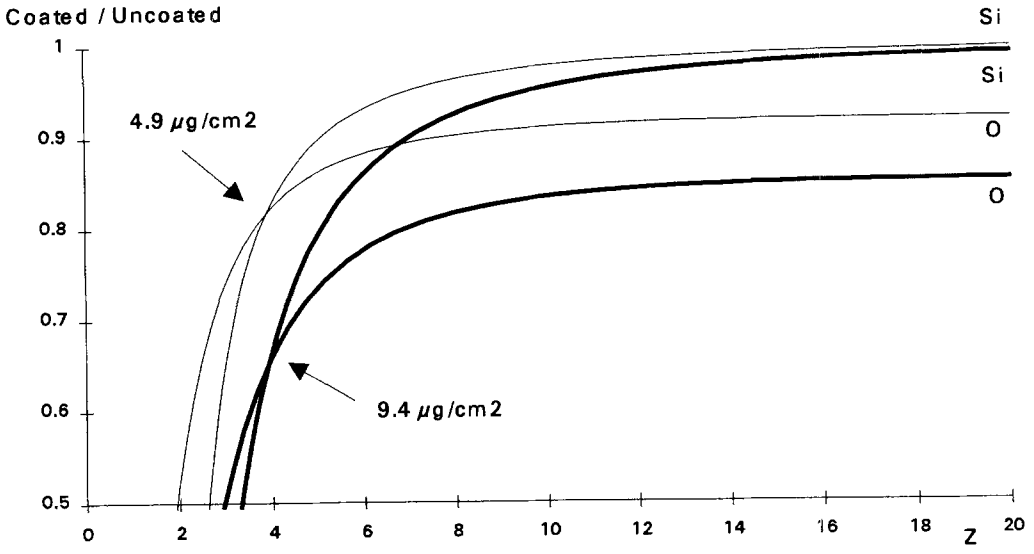

Fig. 9. Influence of carbon coatings (thicknesses 4.9 and 9.4 $\mu g/cm^2$) on the O Kα and Si Kα intensities emitted by SiO_2 as a function of the accelerating voltage. The curves represent the ratio of coated to uncoated specimen intensities. Take-off angle 35°

the k-ratio in standardless analysis. The coating has not the same influence for all the analyzed elements: its effect cannot be neglected for the strongly absorbed radiations (i.e. particularly for the ultra-light elements) and for the elements analyzed at low overvoltage. Figure 9 illustrates the effect of a carbon coating with two different thicknesses (4.9 and 9.4 $\mu g/cm^2$, i.e. ~25 and 47 nm) on the O Kα and Si Kα intensities emitted by a SiO_2 specimen. At the highest accelerating voltages, the effect of the coating is mainly an absorption of the radiation, with is almost negligible for Si Kα (~1% or less in these examples), but which represents ~9 or 16% for O Kα, depending on the carbon thickness. At lower overvoltage, the loss of intensity produced by the coating is more pronounced because the loss of energy of the electrons in the surface film becomes significant. In the present examples, at accelerating voltages lower than ~4 kV, the loss of intensity becomes more important for Si Kα than for O Kα. At ~4 kV, the intensity loss due to the thinner coating is ~17% for both elements, and ~35% for the thicker one.

In the Quantex+/XPP program, we have implemented an option which enables to take into account the influence of the coating on the quantitative analysis. This option can be used when the mass thickness of the coating represents a small fraction of the maximum ionization depth (so that it can be assumed that the $\phi(\rho z)$ function for the coated specimen is the same as that of the uncoated specimen), and when the absorption of the analyzed radiations in the coating are moderate (not more than 25%). The mass thickness of the coating has to be known or has to be measured by X-ray microanalysis, using an appropriate standard (e.g. vitreous carbon in the case of a C coating) and an appropriate thin film program (e.g. *Strata*, *Multifilm*, or other). The computation is executed in two steps: in the first step, the presence of the coating is neglected, and the normal standardless procedure gives a first approximation of the composition of the specimen. In the second step, this composition is

Table 6. Results of standardless analyses of carbon coated SiO_2 obtained by using or not the /COATING option in the Quantex+/XPP program. Coating thicknesses 4.9 and 9.4 $\mu g/cm^2$, determined by applying the *Strata* program to carbon measurements with standard (35° take-off)

		5 kV		10 kV		15 kV		Average [r.m.s.]	
Standardless procedure	C thickness ($\mu g/cm^2$)	Si at. %	O at. %	Si at. %	O at. %	Si at. %	O at. %	Si at. %	O at. %
XPP	4.9	33.20	66.80	34.52	65.48	35.28	64.72	34.97	65.03
	9.4	34.25	65.75	35.88	64.12	36.70	63.30	[1.14]	[1.14]
XPP/COAT	4.9	32.26	67.74	33.18	66.82	33.98	66.02	33.20	66.80
	9.4	32.37	67.63	33.27	66.73	34.16	65.84	[0.72]	[0.72]

used to define the $\phi(\rho z)$ functions needed to evaluate the influence of the coating on every analytical line of the specimen. Table 6 shows in the case of carbon coated SiO_2 that the /COATING option produces an appreciable global improvement of the standardless results.

Stratified Specimens

It it also interesting, mainly for routine control applications, to try to save time in the case of stratified specimens by using a restricted number of standards. In the particular case of stratified specimens, the objective is to obtain both the composition and the thickness of the layers of the specimen. Hence, as opposed to the case of homogeneous volumes where normalized k-ratios can be used, "true" k-ratios are needed in the present case, since the sum of the k-ratios is used to derive the layer thickness. As mentioned in the introduction paragraph, it is very difficult in practice to obtain "true" k-ratios without using a standard. But what can be done is to use a single reference which enables to eliminate all the factors which are not well defined (beam current, solid angle of detection, B_j factor in the ionization cross-section).

Hence, if standardless procedures are not easily applicable to stratified specimens, "as soon as possible" procedures may be effective. Such an ASAP procedure has been implemented in the *Multifilm* software program designed for the Kevex EDS systems. Table 7 shows the application of such a procedure to the analysis of a Co_3Ti compound coated with copper layer of ~ 150 nm. The results of the ASAP procedure using a single Cr reference (element not present in the specimen) are shown to be in satisfactory agreement with the results obtained with standards. The use of several geometrical configurations of analysis illustrates the capability of the technique.

Obviously, the quality of the results of the ASAP procedure applied to stratified specimens depends on the performance of the standardless analysis for the same elements in homogeneous specimens. For example, it would dangerous in the present state of the knowledge to apply an ASAP procedure when L lines are involved, because of the uncertainties due to the radiationless transitions.

Table 7. Results of an ASAP procedure (single Cr reference) compared with results of an analysis with standards in the case of a stratified specimen Cu/Co_3Ti (nominal 20.7 wt % Ti). 15 kV. *Multifilm* program

			With Cu, Co, Ti standards			ASAP, with Cr reference		
Azimuth (deg)	Tilt (deg)	Take-off (deg)	Cu thick. (nm)	Cu wt %	Ti wt %	Cu thick. (nm)	Cu wt %	Ti wt %
0	0	35.0	141	79.1	20.9	—	—	—
0	20	55.0	150	79.5	20.5	163	79.5	20.5
40	20	48.9	142	79.7	20.3	149	79.8	20.2
60	20	42.7	140	80.0	20.0	150	80.0	20.0
80	20	36.0	144	79.6	20.4	149	79.9	20.1
100	20	29.8	147	79.3	20.7	150	79.5	20.4
Average			144	79.5	20.5	152	79.8	20.2
Relative r.m.s.			2.6%	0.4%	1.5%	4.1%	0.3%	1.0%
Deviation from nominal				+0.3%	−1.0%		+0.6%	−2.4%

Conclusion

Significant improvements have been obtained recently in the field of standardless EDS X-ray microanalysis. These improvements are due to the simultaneous amelioration of the detector technology and of the quantitative procedures. Presently, it is possible to obtain in most cases of standardless analyses involving K lines only quite satisfactory results (accuracy of the order of one percent relative for major elements). For the ultra-light elements, the situation is more difficult, both on the experimental and on the theoretical point of view. More work is needed to clarify the situation, but it can be expected that an accuracy better than 5% could be obtained soon. The most urgent problem to solve for being able to use reliably standardless analysis is the problem of the radiationless transitions between L subshells. It is clear that these effects have to be taken into account, but it seems that the theoretical values of the Coster-Kronig probabilities of transition are not able to predict correctly the amplitude of the effects. To perform reliable adjustments of these probabilities, a large and consistent set of data is required.

Provided that advanced $\phi(\rho z)$ models are used, the analysis of tilted specimens can be done without significant loss of accuracy. These models also enable to analyse insulating specimen with a coated surface, and even to characterize more complex stratified specimens, provided that a single reference is measured.

Acknowledgements. The developments in the Kevex sofware have been done in cooperation with SAMx (Support for Applications in X-ray Microanalysis), 4 rue Galilée, 78380 Guyancourt, France, under contract ONERA/SAMx #6361. The author gratefully acknowledges the experimental contribution of D. Boivin (ONERA).

References

[1] J. L. Pouchou, F. Pichoir, *Electron Probe Quantitation* (K. F. J. Heinrich, D. E. Newbury, eds.), Plenum, New York, 1991, pp. 31–75.

[2] R. H. Packwood, *Electron Probe Quantitation* (K. F. J. Heinrich, D. E. Newbury, eds.), Plenum, New York, 1991, pp. 83–104.

[3] G. F. Bastin, H. J. M. Heijligers, *Electron Probe Quantitation* (K. F. J. Heinrich, D. E. Newbury, eds.), Plenum, New York, 1991, pp. 145–161.

[4] J. L. Pouchou, F. Pichoir, *Microbeam Analysis*, San Francisco Press, San Francisco, 1988, pp. 319–324.

[5] W. Bambynek, B. Craseman, R. Fink, H. U. Freund, H. Mark, C. D. Swift, R. E. Price, Rao P. Venugopala, *Rev. Mod. Phys.* **1972**, *44*, 716.

[6] J. Labar, *Scanning Microsc.* in press.

[7] M. O. Krause, *J. Phys. Chem. Ref. Data* **1979**, *8*, 307.